



Metabolic Mitigation of *Staphylococcus aureus* Vancomycin Intermediate-Level Susceptibility

Stewart G. Gardner,^a Darrell D. Marshall,^{b,*} Robert S. Daum,^{c,d,e} Robert Powers,^{b,f} Greg A. Somerville^a

^aSchool of Veterinary Medicine and Biomedical Sciences, University of Nebraska—Lincoln, Lincoln, Nebraska, USA

^bDepartment of Chemistry, University of Nebraska—Lincoln, Lincoln, Nebraska, USA

^cDepartment of Medicine, University of Maryland School of Medicine, Baltimore, Maryland, USA

^dInstitute for Global Health, University of Maryland School of Medicine, Baltimore, Maryland, USA

^eCenter for Vaccine Development, University of Maryland School of Medicine, Baltimore, Maryland, USA

^fNebraska Center for Integrated Biomolecular Communication, University of Nebraska—Lincoln, Lincoln, Nebraska, USA

ABSTRACT *Staphylococcus aureus* is a major human pathogen whose infections are increasingly difficult to treat due to increased antibiotic resistance, including resistance to vancomycin. Vancomycin-intermediate *S. aureus* (VISA) strains develop resistance to vancomycin through adaptive changes that are incompletely understood. Central to this adaptation are metabolic changes that permit growth in the presence of vancomycin. To define the metabolic changes associated with adaptive resistance to vancomycin in *S. aureus*, the metabolomes of a vancomycin-sensitive and VISA strain pair isolated from the same patient shortly after vancomycin therapy began and following vancomycin treatment failure were analyzed. The metabolic adaptations included increases in acetogenesis, carbon flow through the pentose phosphate pathway, wall teichoic acid and peptidoglycan precursor biosynthesis, purine biosynthesis, and decreased tricarboxylic acid (TCA) cycle activity. The significance of these metabolic pathways for vancomycin-intermediate susceptibility was determined by assessing the synergistic potential of human-use-approved inhibitors of these pathways in combination with vancomycin against VISA strains. Importantly, inhibitors of amino sugar and purine biosynthesis acted synergistically with vancomycin to kill a diverse set of VISA strains, suggesting that combinatorial therapy could augment the efficacy of vancomycin even in patients infected with VISA strains.

KEYWORDS *Staphylococcus aureus*, metabolism, physiology, vancomycin resistance

Staphylococcus aureus is the causative agent of many bacterial infections in humans, such as skin and respiratory infections, meningitis, and sepsis. With the rise of antibiotic resistance, treatment of these infections is increasingly difficult. Of particular importance, methicillin-resistant *S. aureus* (MRSA) infections have become a major problem in hospitals and the community. Treatment of serious MRSA infections often involves the antibiotic vancomycin; however, resistance to vancomycin is also increasing (1–5).

Vancomycin inhibits cell wall synthesis by binding to the D-alanyl–D-alanine carboxyl terminus of cell wall precursor molecules, preventing the cross-linking of peptidoglycan (6). Vancomycin-susceptible *S. aureus* (VSSA) strains have a vancomycin MIC of 0.5 to 2 $\mu\text{g}/\text{ml}$, while vancomycin-resistant *S. aureus* (VRSA) strains have acquired resistance genes that confer a MIC of $>16 \mu\text{g}/\text{ml}$. While VRSA isolates are rare, the prevalence of vancomycin-intermediate *S. aureus* (VISA; MIC of 3 to 8 $\mu\text{g}/\text{ml}$) is increasing (5, 7). The most common mechanism by which *S. aureus* acquires intermediate susceptibility to

Received 3 August 2017 Returned for modification 15 September 2017 Accepted 28 October 2017

Accepted manuscript posted online 6 November 2017

Citation Gardner SG, Marshall DD, Daum RS, Powers R, Somerville GA. 2018. Metabolic mitigation of *Staphylococcus aureus* vancomycin intermediate-level susceptibility. *Antimicrob Agents Chemother* 62:e01608-17. <https://doi.org/10.1128/AAC.01608-17>.

Copyright © 2017 American Society for Microbiology. All Rights Reserved.

Address correspondence to Robert Powers, rpowers3@unl.edu, or Greg A. Somerville, gsomerville3@unl.edu.

* Present address: Darrell D. Marshall, Department of Chemistry, Wayne State University, Detroit, Michigan, USA.

S.G.G. and D.D.M. contributed equally to this work.

vancomycin is by adapting its physiology and metabolism to permit growth in the presence of vancomycin, a process known as adaptive resistance. One metabolic adaptation that VISA strains commonly have is an alteration in their ability to catabolize incompletely oxidized carbon sources, such as acetate (8). This adaptation is due in part to a reduction in tricarboxylic acid cycle activity. Because the metabolic adaptations involve central metabolism, it is likely that a broader array of metabolic changes are involved in intermediate-level susceptibility to vancomycin.

S. aureus strains demonstrating an intermediate level of resistance to vancomycin first emerged in Japan in 1996 and the following year in the United States (9–11). These VISA strains had increased cell wall thickness that is thought to limit the access of vancomycin to its target, specifically, the nascent cell wall at the division septum (12–16). Increased cell wall thickness is the most consistent phenotypic change observed in VISA strains (17), while other cell wall changes (e.g., reduced peptidoglycan cross-linking or changes in the levels of penicillin-binding proteins) vary between strains (5). While the phenotype of VISA strains is fairly consistent, the genotypic changes display considerable variation (5). In heterogeneous vancomycin-intermediate *S. aureus* (hVISA) and VISA strains, nonsynonymous single-nucleotide polymorphisms (SNPs) are frequently found in *vraS*, *vraR*, *yvqF* or *vraT*, *walk*, *rpoB*, *graR*, *graS*, and *walR* (18). These genes are members of 2-component (i.e., *walKR* and *graRS*) and 3-component (i.e., *vraTSR*) regulators involved in cell wall biosynthesis and degradation and the alternative sigma factor σ^B (i.e., *rpoB*), which is a stress response sigma factor (5, 18–20). Most clinical VISA isolates have SNPs in one or more of these regulatory components (18); unfortunately, information regarding the contributions of most of these SNPs to metabolic changes is lacking (21). To address this deficiency, the metabolic and physiological differences in the isogenic MRSA clinical isolates Q2275 (VSSA) and Q2283 (VISA) were characterized.

RESULTS

The VISA phenotype decreases growth yield, acetate catabolism, and TCA cycle activity. Previously, we observed that VISA strains were impaired in their ability to catabolize incompletely oxidized carbon compounds (i.e., acetate), which decreased their growth yields relative to those of VSSA strains (8). To establish that this strain pair was consistent with our previous observations, growth was assessed by cultivation of strains Q2275 and Q2283 in tryptic soy broth (TSB) and hourly measurement of the optical density at 600 nm (OD_{600}) and pH of the culture media (Fig. 1A). The two strains had similar doubling times, specifically, 28.4 ± 0.6 min and 27.7 ± 0.5 min for Q2275 and Q2283, respectively. While the growth rates were the same, the growth yield of strain Q2283 was slightly lower than that of strain Q2275 (Fig. 1A). The growth yield difference between the strains was also reflected in pH profile differences of the culture media. These differences are consistent with previous observations (8) and indicate an alteration in post-exponential-phase metabolism in strain Q2283 relative to strain Q2275. To determine if the growth yield and pH profile differences between strains Q2283 and Q2275 were due to differences in acetate accumulation and depletion, acetate concentrations in the cultivation media were determined (Fig. 1B). Consistent with the pH profiles, growth-normalized accumulation of acetate in the culture medium was reduced in strain Q2283 relative to that in strain Q2275. Acetate catabolism requires tricarboxylic acid (TCA) cycle activity and anaplerotic metabolites to offset the efflux of biosynthetic intermediates from the TCA cycle. Commonly, the anaplerotic metabolites are derived from amino acids, leading to the accumulation of ammonia in the cultivation media due to deamination reactions. The rates of ammonia accumulation in the culture media were similar between strains Q2283 and Q2275; however, the greater cell density achieved by strain Q2275 resulted in a greater ammonia concentration than that of strain Q2283 (Fig. 1C). These data are indicative of strain Q2283 having an alteration in TCA cycle activity relative to strain Q2275; hence, the activity of aconitase was assessed (Fig. 1D). In *S. aureus*, TCA cycle activity is largely repressed during exponential growth in nutrient-replete conditions and derepressed during

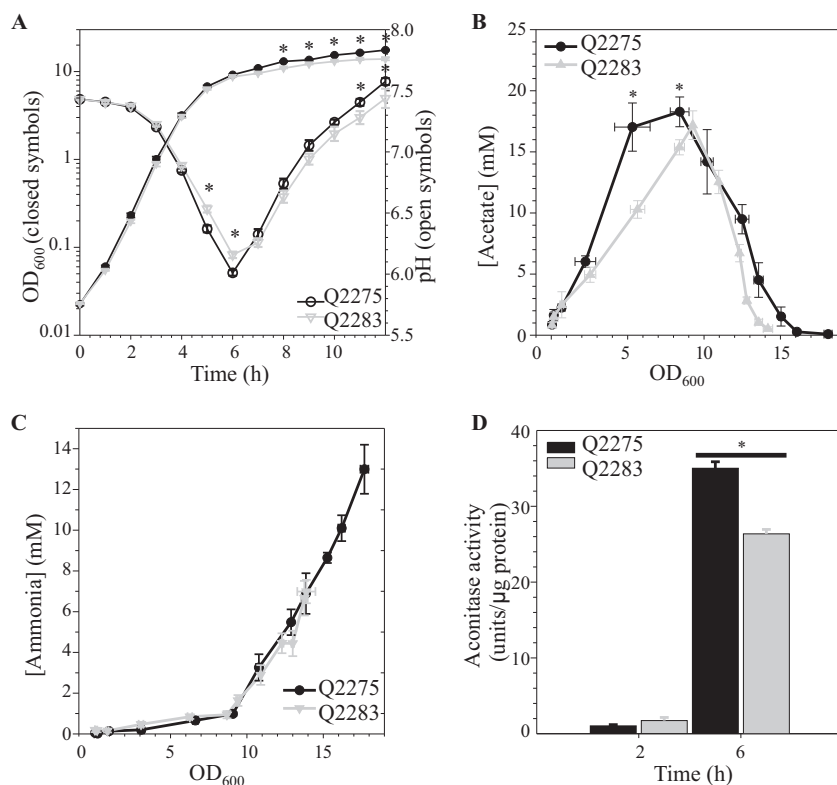


FIG 1 *S. aureus* strain Q2275 and Q2283 growth characteristics and aconitase activity. (A) Strains Q2275 (black circles) and Q2283 (gray triangles) were cultivated as described in the text, and the OD₆₀₀ (closed symbols) and pH (open symbols) of the cultures were determined hourly. Data represent the averages of results from four independent replicates, with error bars indicating the standard error of the mean (SEM). Asterisks represent *P* values of <0.05 based on a two-way ANOVA. Cultivation medium concentrations of acetate (B) and ammonia (C) for cultures of strains Q2275 and Q2283 are plotted as a function of the growth. Values are the mean and SEM from three independent cultures. Asterisks indicate *P* values of <0.05 based on a two-way ANOVA. (D) Aconitase activity was determined in the exponential (2-h)- and post-exponential (6-h)-growth phases for strains Q2275 (black bars) and Q2283 (gray bars). The data shown are the mean and SEM from three independent experiments. Asterisk, *P* < 0.05, calculated with Student's *t* test.

post-exponential-phase growth when carbon is limiting (22). As expected, both strains Q2275 and Q2283 had minimal activity during exponential growth (2 h). During the post-exponential-growth phase (6 h), both strains Q2275 and Q2283 had increased aconitase activity relative to that of the exponential-growth phase; however, strain Q2275 had significantly (*P* < 0.05) more aconitase activity than did strain Q2283. Overall, these data are consistent with a VISA phenotype having decreased acetate catabolism and reduced TCA cycle activity (8).

The VISA metabolome is significantly altered from the VSSA metabolome.

During the post-exponential-growth phase, VISA strain Q2283 had significantly decreased aconitase activity, resulting in a diminished ability to utilize acetate relative to that of the VSSA strain Q2275 (Fig. 1). To determine if these metabolic differences significantly altered the VISA metabolome, 1-dimensional (1D) ¹H nuclear magnetic resonance (NMR) metabolomics was performed on the VSSA and VISA strains during the exponential (2-h)- and post-exponential (6-h)-growth phases and the data were analyzed by principal-component analysis (PCA). The resulting PCA model yielded *R*² and *Q*² values of 0.8328 and 0.5709, respectively, which are consistent with a reliable model (23). As expected, the PCA score plot of the ¹H NMR profiles revealed four distinct clusters. The greatest separation was temporal, due to the differences in the growth phases, followed by separation based on strain phenotype (Fig. 2A). This separation is more easily observed in the dendrogram, which reflects the *P* value

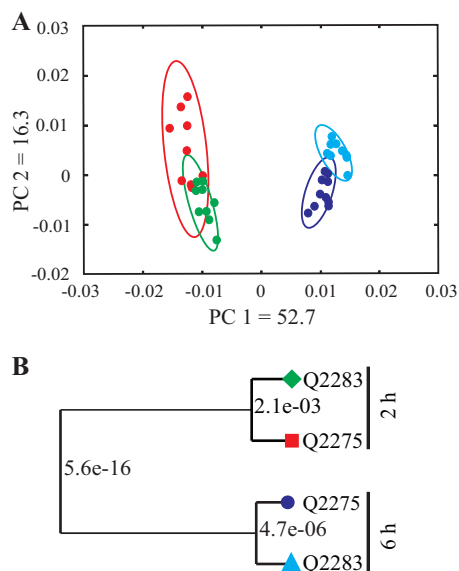


FIG 2 Statistical analysis of 1D ^1H NMR metabolomic samples. Metabolomic analysis of VSSA strain Q2275 and VISA strain Q2283 during the exponential (2-h)- and post-exponential (6-h)-growth phases. (A) 2D PCA score plot comparing the 1D ^1H NMR fingerprints of Q2275 at 2 h (red), Q2283 at 2 h (green), Q2283 at 6 h (blue), and Q2275 at 6 h (purple). Ellipses represent a 95% confidence limit of the normal distribution of each cluster. The PCA model yielded R^2 and Q^2 values of 0.8328 and 0.5709, respectively. (B) Dendrogram generated from PCA score plots, with each Mahalanobis distance P value represented between the nodes.

distance between each node (Fig. 2B). These data demonstrate that the transition to a VISA phenotype is accompanied by significant global metabolic changes in *S. aureus*.

To ascertain the metabolic changes that accompany the transition from a VSSA to a VISA phenotype, orthogonal projections to latent-structure discriminant analysis (OPLS-DA) was performed on the ^1H NMR spectral data for both growth phases (Fig. 2). A valid OPLS-DA model was evident by an R^2 value of 0.9801, a Q^2 value of 0.8977, and a cross-validated analysis of variance (CV-ANOVA) P value of 2.62×10^{-5} . In OPLS-DA, class membership is supervised and variation between two groups is observed by the predictive component (x axis or P_p), while the orthogonal component (y axis or P_o) represents all other variation in the analysis. There were several differences between the strains that were independent of the growth phase, including in their levels of betaine and glycerol, which were increased in VISA, and alanine and branched-chain amino acids (i.e., valine, isoleucine, and leucine), which were increased in VSSA. In contrast, the abundance of several metabolites was temporally altered. As an example, the pseudo-1D ^1H spectra indicate that the concentration of citrate was higher in strain Q2275 during the exponential-growth phase (2 h) but was higher in strain Q2283 during the post-exponential-growth phase (6 h) (Fig. 3). These data indicate that some changes associated with the VISA phenotype are growth phase dependent.

The VISA strain Q2283 increased carbon flow to cell wall precursor biosynthesis relative to that of the VSSA strain Q2275. ^1H NMR analysis of the exponential- and post-exponential-growth-phase metabolomes (Fig. 2) demonstrated that significant metabolic differences exist between strains Q2275 and Q2283. To better characterize these metabolic differences, $[^{13}\text{C}_6]$ glucose and 2-dimensional (2D) ^1H - ^{13}C heteronuclear single-quantum-coherence (HSQC) NMR were used to determine traced metabolic changes. Due to the minimal metabolic perturbations in the exponential-growth phase, these experiments were only performed on post-exponential-growth-phase (6-h) bacterial cultures. The 2D ^1H - ^{13}C HSQC NMR spectral data of the $[^{13}\text{C}_6]$ glucose-labeled metabolites of the VSSA and VISA strains were analyzed by PCA to assess the reliability of the model (Fig. 4A). The resulting PCA model yielded R^2 and Q^2 values of 0.9831 and 0.7819, respectively, which are consistent with a reliable model.

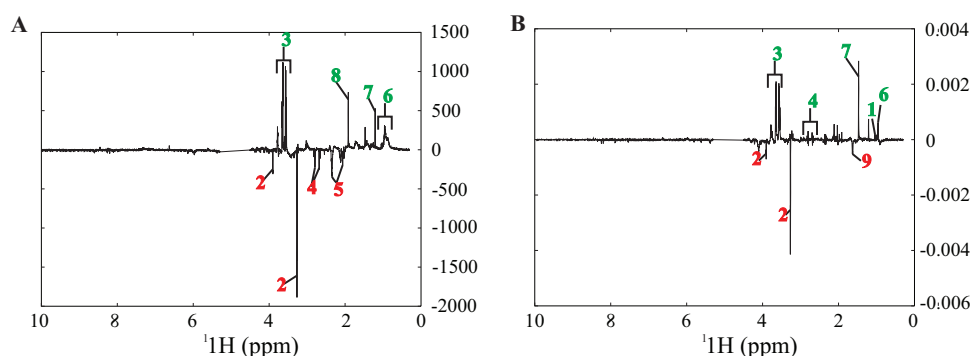


FIG 3 OPLS-DA back-scaled loadings plots for the 2-h (A) and 6-h (B) time points comparing strains Q2275 and Q2283. Peaks pointing down represent an increase in Q2275 and peaks pointing up represent an increase in Q2283 for the pseudo-1D ^1H NMR spectra. OPLS-DA model validation yielded an R^2 of 0.9801, a Q^2 of 0.8977, and a CV-ANOVA P value of 2.62×10^{-5} . Peaks: 1, α -keto-isovalerate; 2, betaine; 3, glycerol; 4, citrate; 5, glutamate; 6, branch-chain amino acids; 7, alanine; 8, acetate; 9, acetyl-phosphate.

As expected, PCA revealed two distinct clusters coinciding with the VISA and VSSA strains. OPLS-DA was then performed on the data, and a valid model was evident by an R^2 value of 0.9831, a Q^2 value of 0.9065, and a CV-ANOVA P value of 2.76×10^{-10} . The OPLS-DA model was used to generate a pseudo-2D HSQC spectrum (back-scaled loadings) (Fig. 4B). Peaks in the spectrum represent metabolites that produced the greatest contribution to the differences between the two strains, including dramatic shifts in the overall distribution of carbon. Specifically, changes were observed in TCA-cycle-derived metabolites, pyrimidine and purine nucleotide intermediates, and arginine- and proline-derived metabolites. To better visualize the relative intensities of the 2D ^1H - ^{13}C HSQC NMR experiments, the data were plotted in a heatmap and bar graphs (Fig. 5 and Fig. 6).

Relative to the VSSA strain Q2275, the VISA strain Q2283 increased its accumulation of glycolytic/gluconeogenesis pathway-associated metabolites, namely, glucose-6-phosphate, fructose-6-phosphate, 3-phosphoglycerate, and phosphoenolpyruvate (PEP). In addition, strain Q2283 shunted more carbon into the pentose phosphate pathway (PPP); this is indicated by the accumulation of the metabolites xylulose 5-phosphate and ribulose-5-phosphate. Consistent with the observation that VISA strains commonly have an increase in cell wall thickness (3), two peptidoglycan precursors, mannose and *N*-acetylglucosamine,

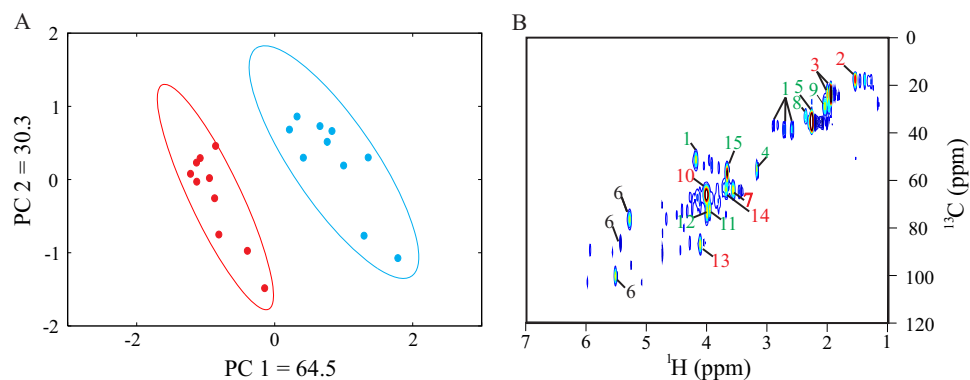


FIG 4 Glucose-derived metabolites identified using 2D ^1H - ^{13}C HSQC NMR. Analysis of 6-h cultures cultivated with media containing ^{13}C -glucose. (A) PCA score plot of 2D ^1H - ^{13}C HSQC NMR data set comparing strains Q2275 (red) and Q2283 (blue). The PCA model yielded R^2 and Q^2 values of 0.9831 and 0.7819, respectively. (B) The corresponding OPLS-DA back-scaled loading plot or pseudo-2D HSQC spectrum (red represents an increase in Q2275 and blue represents an increase in Q2283). OPLS-DA model validation yielded an R^2 of 0.9831, a Q^2 of 0.9065, and a CV-ANOVA P value of 2.76×10^{-10} . Labels are as follows: 1, aspartate; 2, alanine; 3, *N*-acetyl-D-glucosamine; 4, betaine; 5, glutamate; 6, unidentified; 7, melibiose; 8, glutamine; 9, proline; 10, CDP-choline; 11, deoxyadenosine; 12, uridine; 13, UDP-glucose; 14, raffinose; and 15, N6-(1,2-dicarboxyethyl)-AMP.

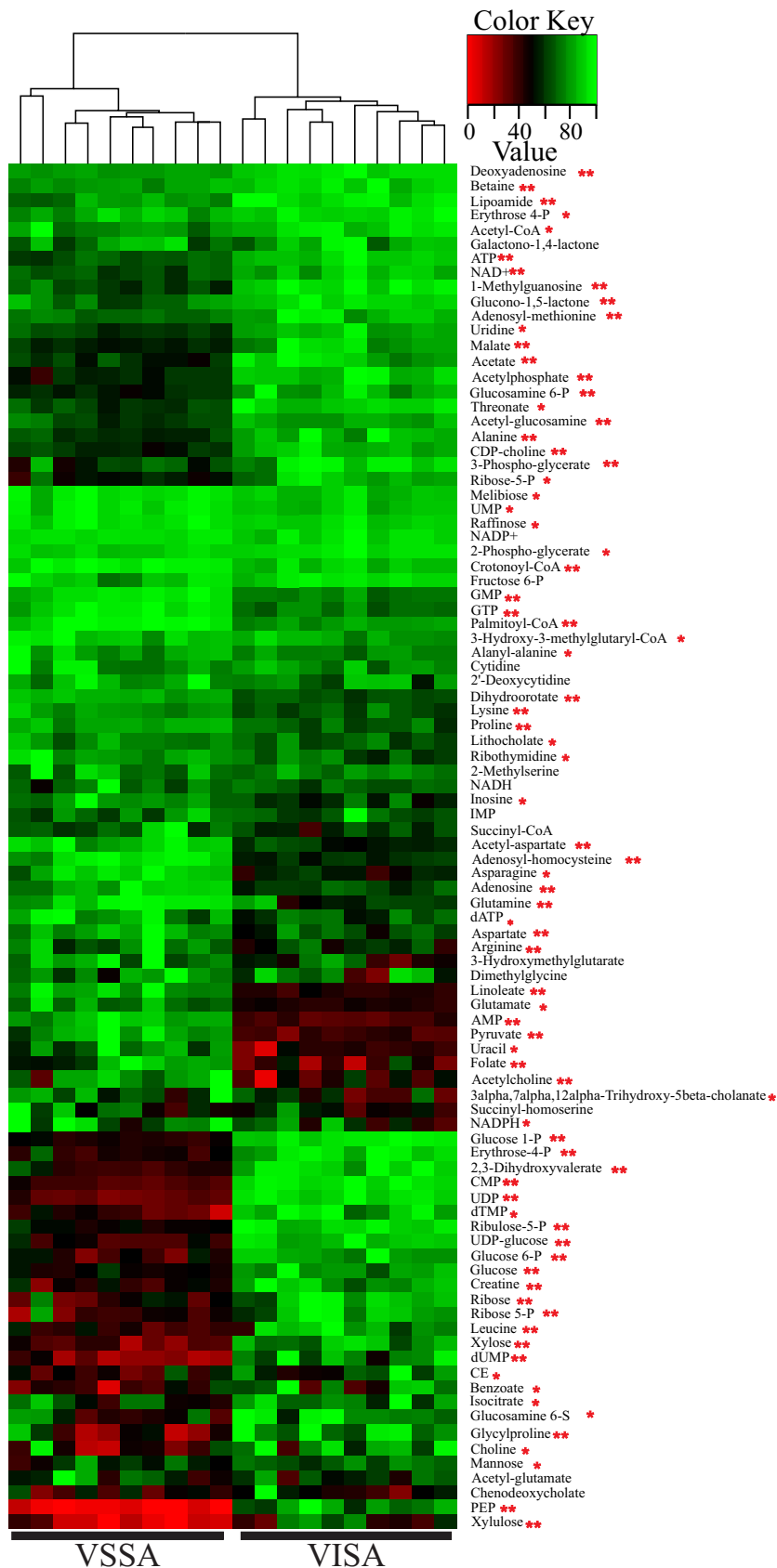


FIG 5 Heatmap showing differences from the VISA metabolome. After 6 h of cultivation, the metabolic changes in VISA strain Q2283 altered the flow of [¹³C]glucose from that of the VSSA strain Q2275. The

(Continued on next page)

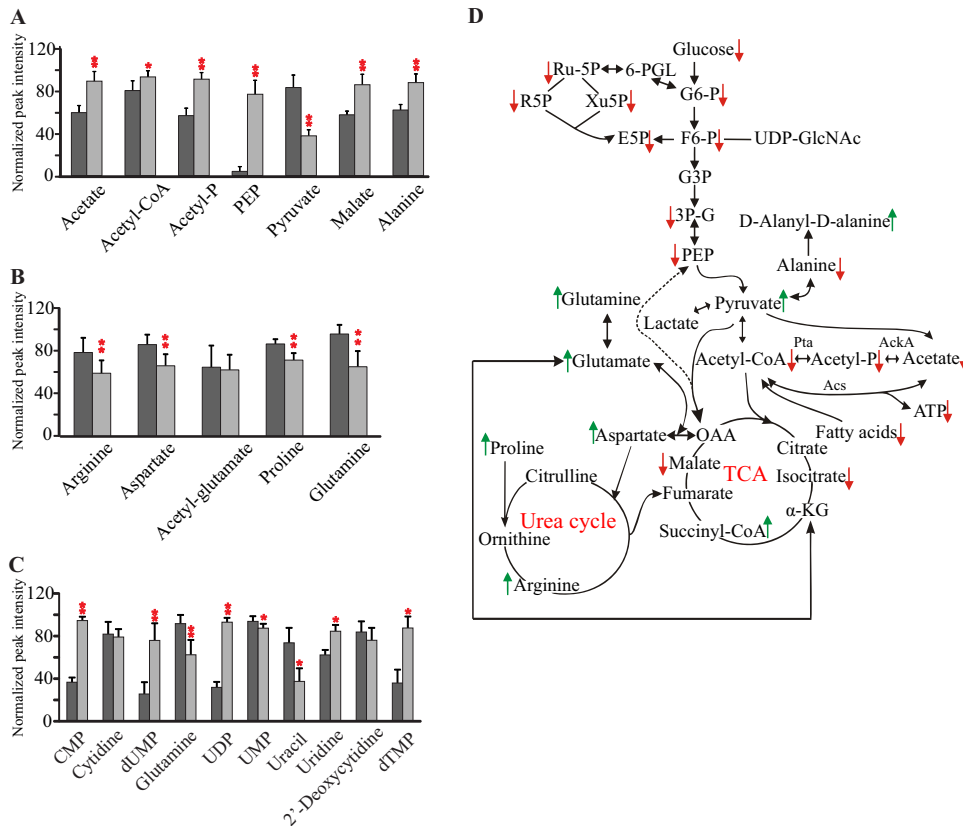


FIG 6 Metabolic changes associated with select pathways. After 6 h of cultivation, VISA strain Q2283 (dark-gray bars) had significantly altered metabolism from that of the VSSA strain Q2275 (light-gray bars). Bar graphs represent 2D ^1H - ^{13}C HSQC NMR analyses ($n = 10$), where the normalized intensities are plotted with the corresponding pathways for central carbon metabolism (A), arginine/proline biosynthesis (B), and purine biosynthesis (C). Statistical significance is denoted by a single asterisk if determined using Student's t test at the 95% confidence level or by two asterisks if determined by Student's t test with a Bonferroni correction for multiple-hypothesis testing (60). (D) Schematic representation of metabolic differences between strains Q2275 and Q2283. Green upward-pointing arrows in the pathways represent a metabolite increase in strain Q2275 relative to the level in strain Q2283, and a downward-pointing red arrow represents a decrease in strain Q2275 relative to the level in strain Q2283. Metabolite abbreviations: acetyl-P, acetyl-phosphate; F6-P, fructose 6-phosphate; G6-P, glucose 6-phosphate; GA3-P, glyceraldehyde 3-phosphate; 3P-G, 3-phosphoglycerate; PEP, phosphoenolpyruvate; Ru5P, ribulose 5-phosphate; Xu5P, xylulose 5-phosphate.

were increased in strain Q2283 relative to the VSSA strain. Interestingly, a decrease in the alanyl-alanine dipeptide (the binding target of vancomycin) was observed in VISA strain Q2283 relative to VSSA strain Q2275. Carbon flux through the phosphotransacetylase-acetate kinase (Pta-AckA) pathway was also increased in VISA strain Q2283, as indicated by increased intracellular accumulation of acetate, acetyl-phosphate, and acetyl coenzyme A (acetyl-CoA). These data suggest that the VISA phenotype coincides with a redirection of carbon into cell wall precursor biosynthesis.

Metabolic inhibitors targeting pathways important for the transition to the VISA phenotype facilitate bacterial killing. The metabolic differences between strains Q2275 and Q2283 provided an opportunity to assess if metabolic inhibitors could be used in combination with vancomycin to enhance killing of VISA and/or VSSA strains. Metabolic data indicated that VISA strain Q2283 had increased purine biosynthesis relative to VSSA

FIG 5 Legend (Continued)

heatmap was generated by using 2D ^1H - ^{13}C HSQC NMR spectrum-normalized peak intensities of the VSSA or VISA strain, and hierarchical clustering is depicted by the dendrogram. The color scale ranges from 0 (red; less intense) to 1 (green; intense). Statistical significance is denoted by a single asterisk if determined using Student's t test at the 95% confidence level or by two asterisks if determined by Student's t test with a Bonferroni correction for multiple-hypothesis testing (60).

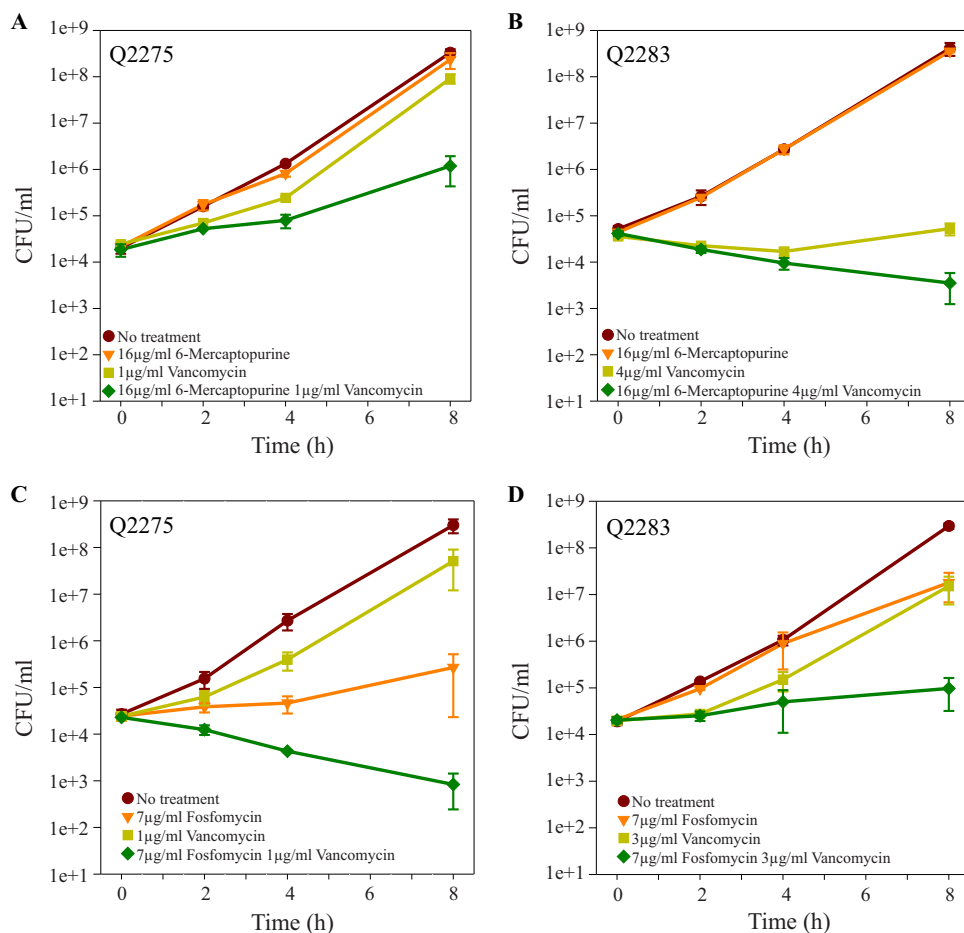


FIG 7 Metabolic inhibitors enhance the efficacy of vancomycin killing of *S. aureus*. Bacteria were cultivated in the presence of metabolic inhibitors (i.e., 6-mercaptopurine and fosfomycin) and vancomycin, and the numbers of CFU per milliliter were determined at 0, 2, 4, and 8 h. Strains Q2275 (A) or Q2283 (B) treated with 6-mercaptopurine and vancomycin. Strain Q2275 (C) or Q2283 (D) treated with fosfomycin and vancomycin. The data shown are the mean and SEM from three independent experiments.

strain Q2275; hence, an inhibitor of purine biosynthesis was chosen for assessing its synergistic potential with vancomycin. Specifically, 6-mercaptopurine was chosen because it is a purine substrate analog, is approved for use in humans, and is occasionally used in the treatment of mycobacterial infections (24–26). At the 16- $\mu\text{g}/\text{ml}$ concentration, 6-mercaptopurine had no effect on bacterial killing of either strain Q2275 or strain Q2283. When combined with sublethal concentrations of vancomycin, 6-mercaptopurine significantly (P values < 0.001) increased staphylococcal killing compared to vancomycin alone (Fig. 7A and B). Another metabolic difference between the strains was an accumulation of phosphoenolpyruvate in the VISA strain relative to the VSSA strain (Fig. 6). As with 6-mercaptopurine, when the PEP substrate analog fosfomycin was used in combination with vancomycin, bacterial killing was dramatically enhanced relative to that with either vancomycin or fosfomycin alone (P values < 0.001) (Fig. 7C and D). These data indicate that it is possible to employ human-use-approved drugs in combination with vancomycin to facilitate *S. aureus* killing, irrespective of susceptibility to vancomycin.

To determine if the 6-mercaptopurine and fosfomycin synergistic effects were specific for this strain pair or more universal, timed killing assays were performed using six VISA strains (i.e., NRS12, NRS17, NRS56, NRS63, NRS118, and HIP5827) (Table 1). Of the strains tested, two of six (i.e., NRS17 and HIP5827) were significantly more susceptible to 6-mercaptopurine and vancomycin than to vancomycin alone (P values < 0.05). All strains except NRS56 were significantly more susceptible to a combination of

TABLE 1 Growth of VISA strains with vancomycin, 6-mercaptopurine, and/or fosfomycin^a

Strain	Condition	Bacterial growth (CFU/ml) at:		P
		0 h	8 h	
NRS12	Medium only	7.87E + 04	8.09E + 08	0.519
	16 μg/ml 6MP	6.68E + 04	6.64E + 08	
	1.25 μg/ml VAN	9.01E + 04	7.83E + 07	
	6MP and VAN	8.24E + 04	2.79E + 07	
	7 μg/ml FOF	6.89E + 04	2.47E + 08	
	FOF and VAN	8.52E + 04	5.90E + 06	
NRS17	Medium only	5.76E + 04	1.69E + 08	0.002
	16 μg/ml 6MP	5.33E + 04	8.14E + 07	
	5 μg/ml VAN	5.19E + 04	2.61E + 05	
	6MP and VAN	4.89E + 04	1.16E + 05	
	7 μg/ml FOF	2.61E + 04	2.14E + 06	
	FOF and VAN	4.03E + 04	1.28E + 04	
NRS56	Medium only	1.51E + 04	2.83E + 07	0.288
	16 μg/ml 6MP	1.49E + 04	1.20E + 07	
	2.5 μg/ml VAN	1.61E + 04	6.15E + 05	
	6MP and VAN	1.25E + 04	3.91E + 05	
	7 μg/ml FOF	1.32E + 04	6.40E + 06	
	FOF and VAN	1.53E + 04	3.03E + 05	
NRS63	Medium only	5.13E + 04	5.01E + 08	0.729
	16 μg/ml 6MP	4.95E + 04	3.86E + 08	
	2.125 μg/ml VAN	5.09E + 04	9.69E + 05	
	6MP and VAN	4.57E + 04	1.32E + 06	
	7 μg/ml FOF	3.45E + 04	8.24E + 07	
	FOF and VAN	3.45E + 04	3.41E + 04	
NRS118	Medium only	5.57E + 04	1.17E + 08	0.628
	16 μg/ml 6MP	5.85E + 04	7.29E + 06	
	2.5 μg/ml VAN	6.31E + 04	8.13E + 05	
	6MP and VAN	5.85E + 04	6.42E + 05	
	7 μg/ml FOF	4.20E + 04	5.87E + 06	
	FOF and VAN	5.56E + 04	2.48E + 04	
HIP5827	Medium only	3.72E + 04	7.91E + 07	<0.001
	16 μg/ml 6MP	3.06E + 04	2.54E + 07	
	1.25 μg/ml VAN	3.59E + 04	3.14E + 06	
	6MP and VAN	3.17E + 04	6.72E + 04	
	7 μg/ml FOF	2.91E + 04	2.57E + 06	
	FOF and VAN	3.77E + 04	7.05E + 03	

^aValues for 0 h and 8 h are the average numbers of CFU per milliliter from three or more replicates, and *P* values are based on two-way ANOVA tests comparing values to those for VAN-treatment-only samples. VAN, vancomycin; 6MP, 6-mercaptopurine; FOF, fosfomycin.

fosfomycin and vancomycin than to vancomycin alone after 8 h (*P* values < 0.05). Taken together, these data suggest that targeting the metabolic adaptations that permit growth in the presence of vancomycin can increase the efficacy of vancomycin, even against VISA strains.

DISCUSSION

S. aureus vancomycin intermediate-level susceptibility arises from genetic and metabolic alterations that result in an increase in cell wall thickness and decreased autolysis (8, 12–17, 27, 28). To ascertain metabolic changes associated with the transition to a VISA phenotype, most studies have used transcriptional and/or proteomic approaches (29–32), while a few studies (21, 33, 34) have taken a direct metabolomic approach to determining metabolic changes associated with the development of the VISA phenotype. To address this deficiency, the metabolic differences between a VSSA and VISA strain pair isolated from a patient shortly after vancomycin treatment began and after treatment failure were assessed. The metabolic adaptations in the VISA strain included an increase in acetogenesis and increases in carbon flow through the pentose phos-

phate pathway, amino sugar precursor biosynthesis, and purine biosynthesis. Consistent with our previous observations, the VISA strain also had decreased carbon flow through the TCA cycle (Fig. 4, 5, and 6). If these metabolic changes are critical for the VSSA to VISA transition, then inhibiting these metabolic pathways could aid in overcoming vancomycin intermediate-level susceptibility. Precedent for this strategy is seen in the two-drug combination of amoxicillin and the β -lactamase inhibitor potassium clavulanate, which was introduced as augmentin in 1981.

The transition to a VISA phenotype altered the availability of PEP and purine biosynthetic intermediates, which suggests that gluconeogenesis and biosynthesis of amino sugars and purine are important for vancomycin intermediate-level susceptibility. Human-use-approved substrate analogs of purines and PEP are available and were used to assess the importance of these metabolic pathways to the VISA phenotype. Specifically, fosfomycin and 6-mercaptopurine were chosen. 6-Mercaptopurine is an inhibitor of purine synthesis that targets hypoxanthine-guanine phosphoribosyltransferase and is used for remission induction and maintenance therapy of acute lymphatic leukemia and Crohn's disease. UDP-*N*-acetylglucosamine enolpyruvyl transferase (MurA) is an enzyme involved in peptidoglycan synthesis and amino sugar recycling that is inhibited by the antimicrobial fosfomycin (35). Interestingly, pyruvate kinase (PykA) is implicated in vancomycin intermediate-level susceptibility and could also be a target of fosfomycin (32, 36). When fosfomycin and 6-mercaptopurine were combined with vancomycin in cultures of strains Q2275 and Q2283, bacterial growth decreased relative to that after use of vancomycin alone, irrespective of vancomycin susceptibility (Fig. 7). Fosfomycin had an inhibitory effect on its own that was enhanced when used in combination with vancomycin for both strains, while 6-mercaptopurine did not significantly affect growth in the absence of vancomycin. These results were expected because the metabolomic data were derived from *S. aureus* strains Q2275 and Q2283. When the same experiment was conducted on a panel of VISA strains (Table 1), the fosfomycin and vancomycin combination proved generally effective at reducing bacterial growth; however, the combination of 6-mercaptopurine and vancomycin was strain dependent. These data provide proof of the concept that metabolic inhibitors combined with vancomycin can resensitize to vancomycin bacteria that have an intermediate level of susceptibility to vancomycin. While this study is limited to human-use-approved drugs that function as metabolic inhibitors, it provides a platform to explore rational drug design for use in combinatorial therapy and to further explore combinatorial possibilities of human-use-approved drugs.

MATERIALS AND METHODS

Bacterial strains. MRSA strains from the same patient were obtained shortly after vancomycin therapy began (Q2275) and after approximately 1 week of vancomycin therapy (Q2283). Q2275 is a VSSA strain (MIC of 2 μ g/ml), while Q2283 is a VISA strain (MIC of 8 μ g/ml). Pulsed-field gel patterns demonstrated that the two strains were from the same clonal complex 5 group, and sequencing at the J. Craig Venter Institute determined them to be identical with the exception of a limited number of SNPs. VISA strains NRS12, NRS17, NRS56, NRS63, and NRS118 were obtained from the Network on Antimicrobial Resistance in *Staphylococcus aureus*, while strain HIP5827 is from Gordon Archer (37).

Bacterial-cultivation conditions. Bacteria were cultivated in filter-sterilized tryptic soy broth (TSB; Becton Dickinson), in TSB without dextrose (Becton Dickinson) supplemented with 0.25% [$^{13}\text{C}_6$]glucose (Cambridge Isotope Laboratories), or on TSB plates containing 1.5% agar. Cultures were inoculated at an optical density at 600 nm (OD_{600}) of 0.01 into prewarmed TSB from a 2-h preculture, using a flask-to-medium ratio of 10:1, and grown at 37°C with 225-rpm aeration. Growth was assessed by hourly measurement of the OD_{600} and pH of the culture.

Growth with vancomycin, fosfomycin, and 6-mercaptopurine. Chemicals were purchased from Sigma (i.e., vancomycin and fosfomycin) or Acros Organics (i.e., 6-mercaptopurine). Bacteria were cultivated in 14-ml culture tubes containing TSB (2 ml) overnight with 225-rpm aeration at a 45-degree angle and at 37°C. Precultures were started by adding 25 μ l of overnight culture to 12.5 ml of TSB in a 125-ml flask and grown for 2 h with 225-rpm aeration at 37°C. Exponential-growth-phase bacterial cultures were diluted in TSB to generate an OD_{600} of 0.08. A total of 10 μ l of these starter cultures was inoculated into 2 ml of TSB containing antibiotics and cultivated with 225-rpm agitation at 37°C. Samples (120 μ l) were collected at 0, 2, 4, and 8 h for determination of numbers of CFU per milliliter. Specifically, 100 μ l of 10-fold serial dilutions in phosphate-buffered saline were spread on TSB agar plates and colonies were counted after 24 h of growth at 37°C. Two-way ANOVA tests on the log numbers of CFU

per milliliter were performed on three independent replicates using SigmaPlot 11.0 for Windows (Systat Software, Inc.).

Measurement of acetate and ammonia concentrations in cultivation media. To determine acetate and ammonia concentrations in the culture media, bacteria (1.5 ml) were harvested by centrifugation for 2 min at $16,100 \times g$ at 4°C, and the supernatants were removed and stored at -20°C until use. Acetate and ammonia concentrations were determined with kits purchased from R-Biopharm and used according to the manufacturer's directions.

Aconitase activity assay. Aconitase activity assays were performed as described previously (38). Bacteria were harvested during exponential growth (2 h) and in the post-exponential-growth phase (6 h) and cell-free lysates were prepared. Results represent the mean and standard deviation of results from three independent experiments.

Nuclear magnetic resonance (NMR) sample preparation. Samples were prepared as described previously, with one alteration (38, 39); to minimize variation due to sample processing and handling, the collection order was randomized.

NMR data collection. Lyophilized cell-free lysates were suspended in 600 μ l of 100% 50 mM D₂O phosphate buffer (uncorrected pH = 7.2) with 50 μ M or 500 μ M 3-(trimethylsilyl) propionic-2,2,3,3-*d*₄ acid sodium salt (TMSP-*d*₄) added for 1D ¹H or 2D ¹H-¹³C HSQC NMR, respectively. 1D and 2D NMR data were collected and processed as described previously (40). Briefly, NMR spectra were collected on a Bruker Avance III-HD700-MHz spectrometer equipped with a quadruple resonance QCI-P cryoprobe (¹H, ¹³C, ¹⁵N, ³¹P), and a SampleJet automated sample changer. All 1D ¹H NMR spectra were collected with an excitation sculpting pulse sequence for solvent suppression (41). Sampling parameters were set to 128 scans, 16 dummy scans, 32,768 data points, a spectral width of 11,160.7 Hz, and a relaxation delay of 1.5 s at 298K. 2D ¹H-¹³C HSQC experiments were carried out with parameters set at 64 scans, 16 dummy scans, 2,048 data points, a spectral width of 11,160.7 Hz, and a relaxation delay of 1.5 s in the ¹H direct dimension and 64 points, with a spectral width of 9,090.9 Hz in the ¹³C indirect dimension.

NMR data processing and analysis. The 1D ¹H NMR and 2D NMR ¹H-¹³C HSQC spectra were processed using the MVAPACK toolbox (<http://bionmr.unl.edu/mvapack.php>) (42). Briefly, 1D ¹H NMR spectra were processed with a 1.0-Hz exponential apodization function and then Fourier transformed. The resulting spectra were simultaneously phased and normalized with phase-scatter correction (PSC) (43) and then referenced to the peak of TMSP-*d*₄ (0.0 ppm). Noise and solvent regions were manually removed. For PCA, the spectral data were binned using the adaptive, intelligent binning algorithm (44), and for OPLS-DA, the full-resolution spectral data were used to build the model. Pareto scaling was applied for both methods.

2D NMR ¹H-¹³C HSQC spectra were processed in MVAPACK with a sine-bell apodization function, zero filled in both dimensions three times, and then Fourier transformed. The resulting spectra were manually phase corrected and standard normal variate (SNV) normalized, and both dimensions were referenced to the peak of TMSP-*d*₄ (0.0 ppm). The spectral data were binned using a generalized adaptive, intelligent binning algorithm (45) and Pareto scaled prior to PCA and OPLS-DA model generation. 2D NMR ¹H-¹³C HSQC spectra were also processed using NMRPipe (46) and NMRViewJ (47) for metabolite assignments. Metabolites were assigned by matching experimental chemical shifts with those from the Platform for Riken Metabolomics (PRIME) database and the Human Metabolome Database (HMDB) (48, 49). Peak error tolerances of 0.08 ppm for ¹H and 0.25 ppm for ¹³C dimensions were used. Metabolite pathway analyses were carried out by identifying the presence of metabolites with the Metacyc database (50), followed by cross-referencing using the MetaboAnalyst (www.metaboanalyst.ca) Web server and the KEGG databases (51–53).

OPLS-DA models were internally cross-validated using 7-fold Monte Carlo cross-validation (54, 55) to compute *Q*² values, which were compared to a distribution of null model *Q*² values in 1,000 rounds of response permutation testing (56). Fractions of explained variation (*R*_x² and *R*_y²) were computed during OPLS-DA model training. Model results were further validated using CV-ANOVA significance testing. Back-scaled loadings plots were generated from OPLS-DA models (57). Ellipses in the PCA and OPLS-DA score plot and the corresponding dendrograms were generated with our PCA/PLS-DA utilities (58, 59) and implemented in MVAPACK (42). The ellipses correspond to the 95% confidence limits from a normal distribution for each group.

ACKNOWLEDGMENTS

This work was supported in part by funding from the Redox Biology Center (P30 GM103335, NIGMS) and the Nebraska Center for Integrated Biomolecular Communication (P20-GM113126, NIGMS), and the research was performed in facilities renovated with support from the National Institutes of Health (RR015468-01). In addition, support was provided by the Nebraska Research Initiative.

We thank Susan Boyle-Vavra for helpful discussions.

REFERENCES

- van Hal SJ, Paterson DL. 2011. Systematic review and meta-analysis of the significance of heterogeneous vancomycin-intermediate *Staphylococcus aureus* isolates. *Antimicrob Agents Chemother* 55:405–410. <https://doi.org/10.1128/AAC.01133-10>.
- Weigel LM, Clewell DB, Gill SR, Clark NC, McDougal LK, Flannagan SE, Kolonay JF, Shetty J, Killgore GE, Tenover FC. 2003. Genetic analysis of a high-level vancomycin-resistant isolate of *Staphylococcus aureus*. *Science* 302:1569–1571. <https://doi.org/10.1126/science.1090956>.

3. Gardete S, Tomasz A. 2014. Mechanisms of vancomycin resistance in *Staphylococcus aureus*. *J Clin Invest* 124:2836–2840. <https://doi.org/10.1172/JCI68834>.
4. Hiramatsu K, Kayayama Y, Matsuo M, Aiba Y, Saito M, Hishinuma T, Iwamoto A. 2014. Vancomycin-intermediate resistance in *Staphylococcus aureus*. *J Glob Antimicrob Resist* 2:213–224. <https://doi.org/10.1016/j.jgar.2014.04.006>.
5. Howden BP, Davies JK, Johnson PDR, Stinear TP, Grayson ML. 2010. Reduced vancomycin susceptibility in *Staphylococcus aureus*, including vancomycin-intermediate and heterogeneous vancomycin-intermediate strains: resistance mechanisms, laboratory detection, and clinical implications. *Clin Microbiol Rev* 23:99–139. <https://doi.org/10.1128/CMR.00042-09>.
6. Reynolds PE. 1989. Structure, biochemistry and mechanism of action of glycopeptide antibiotics. *Eur J Clin Microbiol Infect Dis* 8:943–950. <https://doi.org/10.1007/BF01967563>.
7. Richter SS, Diekema DJ, Heilmann KP, Dohrn CL, Crispell EK, Riahi F, McDanel JS, Satola SW, Doern GV. 2014. Activities of vancomycin, cef-taroline, and mupirocin against *Staphylococcus aureus* isolates collected in a 2011 national surveillance study in the United States. *Antimicrob Agents Chemother* 58:740–745. <https://doi.org/10.1128/AAC.01915-13>.
8. Nelson JL, Rice KC, Slater SR, Fox PM, Archer GL, Bayles KW, Fey PD, Kreiswirth BN, Somerville GA. 2007. Vancomycin-intermediate *Staphylococcus aureus* strains have impaired acetate catabolism: implications for polysaccharide intercellular adhesion synthesis and autolysis. *Antimicrob Agents Chemother* 51:616–622. <https://doi.org/10.1128/AAC.01057-06>.
9. Hiramatsu K, Hanaki H, Ino T, Yabuta K, Oguri T, Tenover FC. 1997. Methicillin-resistant *Staphylococcus aureus* clinical strain with reduced vancomycin susceptibility. *J Antimicrob Chemother* 40:135–136. <https://doi.org/10.1093/jac/40.1.135>.
10. Hiramatsu K, Aritaka N, Hanaki H, Kawasaki S, Hosoda Y, Hori S, Fukuchi Y, Kobayashi I. 1997. Dissemination in Japanese hospitals of strains of *Staphylococcus aureus* heterogeneously resistant to vancomycin. *Lancet* 350:1670–1673. [https://doi.org/10.1016/S0140-6736\(97\)07324-8](https://doi.org/10.1016/S0140-6736(97)07324-8).
11. Centers for Disease Control and Prevention. 1997. *Staphylococcus aureus* with reduced susceptibility to vancomycin—United States, 1997. *MMWR Morb Mortal Wkly Rep* 46:765–766.
12. Cui L, Iwamoto A, Lian J-Q, Neoh H, Maruyama T, Horikawa Y, Hiramatsu K. 2006. Novel mechanism of antibiotic resistance originating in vancomycin-intermediate *Staphylococcus aureus*. *Antimicrob Agents Chemother* 50:428–438. <https://doi.org/10.1128/AAC.50.2.428-438.2006>.
13. Cui L, Murakami H, Kuwahara-Arai K, Hanaki H, Hiramatsu K. 2000. Contribution of a thickened cell wall and its glutamine nonamidated component to the vancomycin resistance expressed by *Staphylococcus aureus* Mu50. *Antimicrob Agents Chemother* 44:2276–2285. <https://doi.org/10.1128/AAC.44.9.2276-2285.2000>.
14. Hanaki H, Kuwahara-Arai K, Boyle-Vavra S, Daum RS, Labischinski H, Hiramatsu K. 1998. Activated cell-wall synthesis is associated with vancomycin resistance in methicillin-resistant *Staphylococcus aureus* clinical strains Mu3 and Mu50. *J Antimicrob Chemother* 42:199–209. <https://doi.org/10.1093/jac/42.2.199>.
15. Hanaki H, Labischinski H, Inaba Y, Kondo N, Murakami H, Hiramatsu K. 1998. Increase in glutamine-non-amidated muropeptides in the peptidoglycan of vancomycin-resistant *Staphylococcus aureus* strain Mu50. *J Antimicrob Chemother* 42:315–320. <https://doi.org/10.1093/jac/42.3.315>.
16. Sieradzki K, Tomasz A. 1999. Gradual alterations in cell wall structure and metabolism in vancomycin-resistant mutants of *Staphylococcus aureus*. *J Bacteriol* 181:7566–7570.
17. Katayama Y, Sekine M, Hishinuma T, Aiba Y, Hiramatsu K. 2016. Complete reconstitution of the vancomycin-intermediate *Staphylococcus aureus* phenotype of strain Mu50 in vancomycin-susceptible *S. aureus*. *Antimicrob Agents Chemother* 60:3730–3742. <https://doi.org/10.1128/AAC.00420-16>.
18. Hafer C, Lin Y, Kornblum J, Lowy FD, Uhlemann A-C. 2012. Contribution of selected gene mutations to resistance in clinical isolates of vancomycin-intermediate *Staphylococcus aureus*. *Antimicrob Agents Chemother* 56:5845–5851. <https://doi.org/10.1128/AAC.01139-12>.
19. Boyle-Vavra S, Yin S, Jo DS, Montgomery CP, Daum RS. 2013. *VraT/VyqF* is required for methicillin resistance and activation of the *VraSR* regulon in *Staphylococcus aureus*. *Antimicrob Agents Chemother* 57:83–95. <https://doi.org/10.1128/AAC.01651-12>.
20. Alam MT, Petit RA, Crispell EK, Thornton TA, Conneely KN, Jiang Y, Satola SW, Read TD. 2014. Dissecting vancomycin-intermediate resistance in *Staphylococcus aureus* using genome-wide association. *Genome Biol Evol* 6:1174–1185. <https://doi.org/10.1093/gbe/evu092>.
21. Alexander EL, Gardete S, Bar HY, Wells MT, Tomasz A, Rhee KY. 2014. Intermediate-type vancomycin resistance (VISA) in genetically-distinct *Staphylococcus aureus* isolates is linked to specific, reversible metabolic alterations. *PLoS One* 9:e97137. <https://doi.org/10.1371/journal.pone.0097137>.
22. Richardson AR, Somerville GA, Sonenshein AL, Sonenshein AL. 2015. Regulating the intersection of metabolism and pathogenesis in gram-positive bacteria, p 129–165. *In* Conway T, Cohen P (ed), *Metabolism and bacterial pathogenesis*. ASM Press, Washington, DC.
23. Worley B, Powers R. 2012. Multivariate analysis in metabolomics. *Curr Metabolomics* 1:92–107. <https://doi.org/10.2174/2213235X11301010092>.
24. Greenstein RJ, Su L, Haroutunian V, Shahidi A, Brown ST. 2007. On the action of methotrexate and 6-mercaptopurine on *M. avium* subspecies *paratuberculosis*. *PLoS One* 2:e161. <https://doi.org/10.1371/journal.pone.0000161>.
25. Shin SJ, Collins MT. 2008. Thiopurine drugs azathioprine and 6-mercaptopurine inhibit *Mycobacterium paratuberculosis* growth *in vitro*. *Antimicrob Agents Chemother* 52:418–426. <https://doi.org/10.1128/AAC.00678-07>.
26. Zimmerman E, Magasanik B. 1964. Utilization and interconversion of purine bases and ribonucleosides by *Salmonella typhimurium*. *J Biol Chem* 239:293–300.
27. Sieradzki K, Tomasz A. 1997. Inhibition of cell wall turnover and autolysis by vancomycin in a highly vancomycin-resistant mutant of *Staphylococcus aureus*. *J Bacteriol* 179:2557–2566. <https://doi.org/10.1128/jb.179.8.2557-2566.1997>.
28. Utaida S, Pfeltz RF, Jayaswal RK, Wilkinson BJ. 2006. Autolytic properties of glycopeptide-intermediate *Staphylococcus aureus* Mu50. *Antimicrob Agents Chemother* 50:1541–1545. <https://doi.org/10.1128/AAC.50.4.1541-1545.2006>.
29. Tan X-E, Neoh H, Looi M-L, Chin SF, Cui L, Hiramatsu K, Hussin S, Jamal R. 2017. Activated ADI pathway: the initiator of intermediate vancomycin resistance in *Staphylococcus aureus*. *Can J Microbiol* 63:260–264. <https://doi.org/10.1139/cjm-2016-0439>.
30. Kuroda M, Kuwahara-Arai K, Hiramatsu K. 2000. Identification of the up- and down-regulated genes in vancomycin-resistant *Staphylococcus aureus* strains Mu3 and Mu50 by cDNA differential hybridization method. *Biochem Biophys Res Commun* 269:485–490. <https://doi.org/10.1006/bbrc.2000.2277>.
31. Mongodin E, Finan J, Climo MW, Rosato A, Gill S, Archer GL. 2003. Microarray transcription analysis of clinical *Staphylococcus aureus* isolates resistant to vancomycin. *J Bacteriol* 185:4638–4643. <https://doi.org/10.1128/JB.185.15.4638-4643.2003>.
32. Howden BP, Smith DJ, Mansell A, Johnson PD, Ward PB, Stinear TP, Davies JK. 2008. Different bacterial gene expression patterns and attenuated host immune responses are associated with the evolution of low-level vancomycin resistance during persistent methicillin-resistant *Staphylococcus aureus* bacteraemia. *BMC Microbiol* 8:39. <https://doi.org/10.1186/1471-2180-8-39>.
33. Dörries K, Schlueter R, Lalk M. 2014. Impact of antibiotics with various target sites on the metabolome of *Staphylococcus aureus*. *Antimicrob Agents Chemother* 58:7151–7163. <https://doi.org/10.1128/AAC.03104-14>.
34. Hattangady D, Singh A, Muthaiyan A, Jayaswal R, Gustafson J, Ulanov A, Li Z, Wilkinson B, Pfeltz R. 2015. Genomic, transcriptomic and metabolomic studies of two well-characterized, laboratory-derived vancomycin-intermediate *Staphylococcus aureus* strains derived from the same parent strain. *Antibiotics* 4:76–112. <https://doi.org/10.3390/antibiotics4010076>.
35. Kahan FM, Kahan JS, Cassidy PJ, Kropp H. 1974. The mechanism of action of fosfomycin (phosphonomycin). *Ann N Y Acad Sci* 235:364–386. <https://doi.org/10.1111/j.1749-6632.1974.tb43277.x>.
36. Matsuo M, Cui L, Kim J, Hiramatsu K. 2013. Comprehensive identification of mutations responsible for heterogeneous vancomycin-intermediate *Staphylococcus aureus* (hVISA)-to-VISA conversion in laboratory-generated VISA strains derived from hVISA clinical strain Mu3. *Antibiotics* 4:76–112. <https://doi.org/10.3390/antibiotics4010076>.
37. Climo MW, Patron RL, Archer GL. 1999. Combinations of vancomycin and beta-lactams are synergistic against staphylococci with reduced susceptibilities to vancomycin. *Antimicrob Agents Chemother* 43:1747–1753.
38. Gaupp R, Lei S, Reed JM, Peisker H, Boyle-Vavra S, Bayer AS, Bischoff M, Herrmann M, Daum RS, Powers R, Somerville GA. 2015. *Staphylococcus aureus* metabolic adaptations during the transition from a daptomycin susceptibility phenotype to a daptomycin nonsusceptibility phenotype. *Antimicrob Agents Chemother* 59:4226–4238. <https://doi.org/10.1128/AAC.00160-15>.
39. Somerville GA, Powers R. 2014. Growth and preparation of *Staphylococ-*

- cus epidermidis* for NMR metabolomic analysis. *Methods Mol Biol* 1106: 71–91. https://doi.org/10.1007/978-1-62703-736-5_6.
40. Halouska S, Zhang B, Gaupp R, Lei S, Snell E, Fenton RJ, Barletta RG, Somerville GA, Powers R. 2013. Revisiting protocols for the NMR analysis of bacterial metabolomes. *J Integr OMICS* 3:120–137.
 41. Nguyen BD, Meng X, Donovan KJ, Shaka AJ. 2007. SOGGY: solvent-optimized double gradient spectroscopy for water suppression. A comparison with some existing techniques. *J Magn Reson* 184: 263–274. <https://doi.org/10.1016/j.jmr.2006.10.014>.
 42. Worley B, Powers R. 2014. MVAPACK: a complete data handling package for NMR metabolomics. *ACS Chem Biol* 9:1138–1144. <https://doi.org/10.1021/cb4008937>.
 43. Worley B, Powers R. 2014. Simultaneous phase and scatter correction for NMR datasets. *Chemom Intell Lab Syst* 131:1–6. <https://doi.org/10.1016/j.chemolab.2013.11.005>.
 44. De Meyer T, Sinnaeve D, Van Gasse B, Tsiorkova E, Rietzschel ER, De Buyzere ML, Gillebert TC, Bekeert S, Martins JC, Van Criekinge W. 2008. NMR-based characterization of metabolic alterations in hypertension using an adaptive, intelligent binning algorithm. *Anal Chem* 80: 3783–3790. <https://doi.org/10.1021/ac7025964>.
 45. Worley B, Powers R. 2015. Generalized adaptive intelligent binning of multiway data. *Chemom Intell Lab Syst* 146:42–46. <https://doi.org/10.1016/j.chemolab.2015.05.005>.
 46. Delaglio F, Grzesiek S, Vuister GW, Zhu G, Pfeifer J, Bax A. 1995. NMRPipe: a multidimensional spectral processing system based on UNIX pipes. *J Biomol NMR* 6:277–293. <https://doi.org/10.1007/BF00197809>.
 47. Johnson BA. 2004. Using NMRView to visualize and analyze the NMR spectra of macromolecules. *Methods Mol Biol* 278:313–352. <https://doi.org/10.1385/1-59259-809-9:313>.
 48. Akiyama K, Chikayama E, Yuasa H, Shimada Y, Tohge T, Shinozaki K, Hirai MY, Sakurai T, Kikuchi J, Saito K. 2008. PRIME: a Web site that assembles tools for metabolomics and transcriptomics. *In Silico Biol* 8:339–345.
 49. Wishart DS, Knox C, Guo AC, Eisner R, Young N, Gautam B, Hau DD, Psychogios N, Dong E, Bouatra S, Mandal R, Sinelnikov I, Xia J, Jia L, Cruz JA, Lim E, Sobsey CA, Shrivastava S, Huang P, Liu P, Fang L, Peng J, Fradette R, Cheng D, Tzur D, Clements M, Lewis A, De Souza A, Zuniga A, Dawe M, Xiong Y, Clive D, Greiner R, Nazyrova A, Shaykhtudinov R, Li L, Vogel HJ, Forsythe I. 2009. HMDB: a knowledgebase for the human metabolome. *Nucleic Acids Res* 37:D603–D610. <https://doi.org/10.1093/nar/gkn810>.
 50. Caspi R, Altman T, Billington R, Dreher K, Foerster H, Fulcher CA, Holland TA, Keseler IM, Kothari A, Kubo A, Krummenacker M, Latendresse M, Mueller LA, Ong Q, Paley S, Subhraveti P, Weaver DS, Weerasinghe D, Zhang P, Karp PD. 2014. The MetaCyc database of metabolic pathways and enzymes and the BioCyc collection of Pathway/Genome Databases. *Nucleic Acids Res* 42:D459–D471. <https://doi.org/10.1093/nar/gkt1103>.
 51. Xia J, Sinelnikov IV, Han B, Wishart DS. 2015. MetaboAnalyst 3.0—making metabolomics more meaningful. *Nucleic Acids Res* 43: W251–W257. <https://doi.org/10.1093/nar/gkv380>.
 52. Kanehisa M, Goto S. 2000. KEGG: kyoto encyclopedia of genes and genomes. *Nucleic Acids Res* 28:27–30. <https://doi.org/10.1093/nar/28.1.27>.
 53. Kanehisa M, Sato Y, Kawashima M, Furumichi M, Tanabe M. 2016. KEGG as a reference resource for gene and protein annotation. *Nucleic Acids Res* 44:D457–D462. <https://doi.org/10.1093/nar/gkv1070>.
 54. Shao J. 1993. Linear model selection by cross-validation. *J Am Stat Assoc* 88:486–494. <https://doi.org/10.1080/01621459.1993.10476299>.
 55. Xu Q-S, Liang Y-Z, Du Y-P. 2004. Monte Carlo cross-validation for selecting a model and estimating the prediction error in multivariate calibration. *J Chemom* 18:112–120. <https://doi.org/10.1002/cem.858>.
 56. Westerhuis JA, Hoefsloot HCJ, Smit S, Vis DJ, Smilde AK, van Velzen EJJ, van Duijnhoven JPM, van Dorsten FA. 2008. Assessment of PLS-DA cross validation. *Metabolomics* 4:81–89. <https://doi.org/10.1007/s11306-007-0099-6>.
 57. Eriksson L, Trygg J, Wold S. 2008. CV-ANOVA for significance testing of PLS and OPLS models. *J Chemom* 22:594–600. <https://doi.org/10.1002/cem.1187>.
 58. Worley B, Halouska S, Powers R. 2013. Utilities for quantifying separation in PCA/PLS-DA scores plots. *Anal Biochem* 433:102–104. <https://doi.org/10.1016/j.ab.2012.10.011>.
 59. Werth MT, Halouska S, Shortridge MD, Zhang B, Powers R. 2010. Analysis of metabolomic PCA data using tree diagrams. *Anal Biochem* 399: 58–63. <https://doi.org/10.1016/j.ab.2009.12.022>.
 60. Noble WS. 2009. How does multiple testing correction work? *Nat Biotechnol* 27:1135–1137. <https://doi.org/10.1038/nbt1209-1135>.